Photoelectron Angular Distribution in Valence Shell Ionization of Heteroaromatic Molecules Studied by the Continuum Multiple Scattering Xα Method

Yoshi-ichi Suzuki and Toshinori Suzuki*

Chemical Dynamics Laboratory, RIKEN, Wako 351-0198, Japan

Received: September 3, 2007

Photoelectron angular distributions are calculated for the valence shell ionization of heteroaromatic molecules of pyridine, pyrazine, pyrimidine, pyrrole, and furan by the continuum multiple scattering Xα method. The asymmetry parameters exhibit strong energy dependences in ionization from π orbitals but are almost invariant in ionization from σ orbitals, in good agreement with experimental results. The asymmetry parameters in ionization from nonbonding orbitals appear generally higher than those in ionization from bonding orbitals. These features are interpreted in terms of the Coulomb phase and photoelectron angular distribution in the molecular frame.

1. Introduction

The one-photon ionization of randomly oriented molecules with linearly polarized light provides a photoelectron angular distribution characterized by a single asymmetry parameter $\beta(E)(-1 \le \beta(E) \le 2)$.[1] This parameter varies with photoionization excess energy depending on the nature of the ionized orbital. For instance, β gradually increases with energy in ionization from π orbitals, but it stays almost constant in ionization from σ orbitals. Although this empirical relation has helped assigning π and σ bands [2−6] in ultraviolet photoelectron spectroscopy (UPS), the origins of such energy dependences have not been elucidated. In this work, we theoretically studied the energy dependence of asymmetry parameters in the photoionization of heteroaromatic molecules with π, σ, and n (nonbonding) electrons. These molecules can also be considered as models of more complex systems of DNA bases[7] that are interesting from a biological viewpoint.

Computational demands are obstacles for detailed studies on photoionization dynamics of polyatomic molecules. To overcome the difficulty and facilitate the analysis, we employ the continuum multiple scattering (CMS) Xα method using muffin-tin potentials for calculating electron scattering waves in the molecular frame (MF). Although the CMSXα method may be less accurate than the *R*-matrix[8] and Schwinger variational methods,[9] previous studies have shown that asymmetry parameters calculated by the CMSXα method agree with experimental values within 0.3 for linear molecules[10−13] and benzene.[14] That level of accuracy would be sufficient for the present study to elucidate differences in ionization from σ (n) and π orbitals semiquantitatively.

Heteroaromatic molecules of pyrazine, pyrimidine, pyridine, furan, and pyrrole are planar with three doubly occupied π orbitals. In the present work, we focus on three types of orbital that correlate with the $1e_{1g}(\pi)$, $3e_{2g}(\sigma)$, and $3e_{1u}(\sigma)$ orbitals in benzene to examine the energy dependences of photoionization asymmetry parameters for these types of orbital systematically. We do not consider orbitals that largely deviate in shape from those in benzene, as their characteristics are determined for some additional factors in individual cases.

2. Theory

The differential cross section in photoionization of an isotropic ensemble of molecules by linearly polarized light takes the following form[1]

$$\frac{d\sigma(E)}{d\Omega} = \frac{\sigma(E)}{4\pi}[1 + \beta(E)P_2(\cos\theta_k)] \tag{1}$$

where $\sigma(E)$ is an integral cross section, $\beta(E)$ is an asymmetry parameter, $P_K(x)$ is the Legendre polynomial of the Kth order, and θ_k is the angle between the photoelectron k-vector and the polarization direction of light. The differential cross section can be expanded in terms of transition dipole moments $I_{lm\mu}(E)$[15] as

$$\frac{d\sigma(E)}{d\Omega} = 4\pi^2 a\hbar\omega/3\sum_{j_t m_t}\sum_{lm\mu l'm'\mu'} i^{l'-l} e^{i(\eta_l(E)-\eta_{l'}(E))} I_{lm\mu}(E)\, I^*_{l'm'\mu'}(E) \times \sum_{K=0,2}(-1)^{\mu+\mu'+j_t}\sqrt{(2l+1)(2l'+1)}P_K(\cos\theta_k)\begin{Bmatrix}1 & 1 & K\\ l & l' & j_t\end{Bmatrix} \times (1-\mu lm|j_t m_t)(1-\mu' l'm'|j_t m_t)(l0l'0|K0)(1010|K0) \tag{2}$$

where a is the fine-structure constant, $\hbar\omega$ is the photon energy, (l,m) are the angular momentum quantum numbers of a partial wave, μ is the index for the dipole moment direction in the molecular frame, $\eta_l(E)$ is the Coulomb phase shift, and $(l_1m_1l_2m_2|LM)$ and $\{:::\}$ are the Clebsch−Gordan coefficient and Wigner 6*j*-symbol, respectively. Comparing eqs 1 and 2, an asymmetry parameter is expressed as[13,15]

$$\beta(E) = \frac{T_2(E)}{T_0(E)} \tag{3}$$

$$T_K(E) = \sum_{j_t ll'}\sqrt{(2l+1)}\sqrt{(2l'+1)}(l0l'0|K0)(1010|K0) \times \begin{Bmatrix}1 & 1 & K\\ l & l' & j_t\end{Bmatrix}(-1)^{j_t} i^{l'-l} e^{i(\eta_l(E)-\eta_{l'}(E))}\sum_{m_t} d_{j_t m_t l}(E)\, d^*_{j_t m_t l'}(E) \tag{4}$$

$$d_{j_t m_t l}(E) = \sum_{m\mu}(-1)^{\mu}(1-\mu lm|j_t m_t)I_{lm\mu}(E) \tag{5}$$

* Corresponding author. E-mail: toshisuzuki@riken.jp.

10.1021/jp077064h CCC: $40.75
Published on Web 01/03/2008

$d_{j_t m_t l}(E)$ is called the reduced amplitude. The energy dependence of $\beta(E)$ arises from the variation in the transition dipole moments (defined as complex values including dynamical phase shifts) and the difference in generic Coulomb phases, $\eta_l(E) - \eta_{l'}(E)$. The latter takes the simple form[16]

$$\eta_l(E) - \eta_{l'}(E) = \sum_{\lambda=l+1}^{l'} \arctan\left(\frac{1}{k\lambda}\right) \qquad (l < l') \tag{6}$$

where $k = \sqrt{2E}$ is the wave number of a photoelectron and E is the photoionization excess energy ($E = \hbar\omega - \mathrm{IE}$). The Coulomb phase difference between the partial waves varies rapidly in the low-energy region up to ca. 5 eV, as k appears as a denominator in (6). Equation 3 can be expanded in terms of the Coulomb phase as[10]

$$\beta(E) = A_0(E) - \sum_{l=1} A_l(E) \cos[\eta_{l_-}(E) - \eta_{l_+}(E) + \Xi_{l_-l_+}(E)\pi] \tag{7}$$

$$\Xi_{l_-l_+}(E)\pi = \arg[\sum_{m_t} d_{lm_t,l-1} d^*_{lm_t,l+1}] \tag{8}$$

where $A_l(E)$ and $\Xi_{l-l_+}(E)$, $l_\pm = l \pm 1$, are the real functions of energy. We used the selection rule of the Clebsch-Gordan coefficient in (4) to obtain (8). Note that the parameters in (7) lack the index of the magnetic quantum number and, therefore, are invariant under the rotation of molecular axes. This axis independence allows an arbitrary choice of the molecular z-axis in treating nonlinear molecules with various symmetries. On the basis of transferred angular momentum formalism,[17,18] A_0 can be written as

$$A_0(E) = \frac{\sum_{j_t}[\sigma_f(j_t)\, B_0(j_t) - \sigma_u(j_t)]}{\sum_{j_t}[\sigma_f(j_t) + \sigma_u(j_t)]} \tag{9}$$

with parity-favored (σ_f) and parity-unfavored (σ_u) terms,

$$\sigma_f(j_t) = S_{j_t j_t - 1} + S_{j_t j_t + 1} \tag{10}$$

$$\sigma_u(j_t) = S_{j_t j_t} \tag{11}$$

$$S_{j_t l} = \sum_{m_t} |d_{j_t m_t l}(E)|^2 \tag{12}$$

and

$$B_0(j_t) = \frac{(j_t - 1)S_{j_t j_t - 1} + (j_t + 2)S_{j_t j_t + 1}}{(2j_t + 1)\sigma_f(j_t)} \tag{13}$$

In contrast to atoms,[1] there are parity-unfavored terms in eq 9, by which $A_0(E)$ can be negative for molecules. $A_0(E)$ can take limiting values 2 and -1 in restrictive situations. From eqs 9 and 13, we can see that the condition for $A_0 = 2$ is $S_{j_t l} \equiv 0$ for all (j_t, l) except S_{01} and that for $A_0 = -1$ is $S_{j j_t \pm 1} \equiv 0$ for all j_t. There is a familiar example of the former, i.e., the atomic ns $\rightarrow$ kp ionization. Those limiting cases are not likely for polyatomic molecules, especially the latter case.

$A_l(E)$, $l \geq 1$, is described as the magnitude of an interference term between the channels with angular momentum $l - 1$ (kl_-) and $l + 1$ (kl_+) and written as

$$A_l = \frac{6\sqrt{l(l+1)}|\sum_{m_t} d_{lm_t l_-} d^*_{lm_t l_+}|}{(2l+1)\sum_{j_t}[\sigma_f(j_t) + \sigma_u(j_t)]} \tag{14}$$

Because the numerator of this equation can be recognized as an inner product, the upper bound for $A_l(E)$ can be derived by the inequality $|\boldsymbol{a}\cdot\boldsymbol{b}^*| \leq |\boldsymbol{a}||\boldsymbol{b}|$.

$$A_l \leq \frac{6\sqrt{l(l+1)S_{ll_-}S_{ll_+}}}{(2l+1)\sum_{j_t}[\sigma_f(j_t) + \sigma_u(j_t)]} \tag{15}$$

which clearly indicates that $A_l(E)$ approaches zero when the ionization into either kl_- or kl_+ continuum becomes negligible.

2.1. Eigenchannel and Eigenphase. In the one-electron approximation, a transition dipole moment is given by

$$I_{lm\mu} = \langle \psi^-_{lm} | r Y_{1\mu} | \phi_0 \rangle \tag{16}$$

where ψ^-_{lm} is the S-matrix-normalized continuum wave function obtained by the CMSXα method[15] and ϕ_0 is an ionized one-electron orbital. The asymptotic form of ψ^-_{lm} is

$$\psi^-_{lm}(r,\theta,\phi,k) \sim \frac{1}{2ir}\sqrt{\frac{1}{k\pi}}[e^{i\omega_l} Y_{lm}(\theta,\phi) - \sum_{l'm'} S^*_{lml'm'} e^{-i\omega_l} Y_{l'm'}(\theta,\phi)] \tag{17}$$

$$\omega_l = kr + \frac{1}{k}\ln(2kr) - \frac{1}{2}l\pi + \eta_l(E) \tag{18}$$

where the $S_{lml'm'}$ is the element of the **S** matrix and the angles θ and ϕ are defined in the molecular frame. The continuum wave function around the shape resonance is analyzed using the eigenphase and eigenchannel formalism. The eigenphases δ_γ are obtained by diagonalizing the **S** matrix as

$$\mathbf{S} = \mathbf{U}\exp(2i\boldsymbol{\delta})\mathbf{U}^\dagger \tag{19}$$

where **U** is the unitary matrix, which consists of column eigenvectors of the **S** matrix, and $\boldsymbol{\delta}$ is the diagonal eigenphase matrix.

Eigenchannel wave functions are obtained by the unitary transformation of the S-matrix-normalized wave functions. The asymptotic eigenchannel functions are expanded by phase-shifted Coulomb wave functions[19,20] as

$$\xi_\gamma(r,\theta\,\phi,k) = e^{i\delta_\gamma} \sum_{L=\{l,m\}} U^*_{L\gamma}\psi^-_{lm}(r,\theta,\phi,k) \tag{20}$$

$$\sim \frac{1}{r}\sqrt{\frac{1}{\pi k}}\sum_L U^*_{L\gamma} Y_{lm}(\theta,\phi)\sin(\delta_\gamma + \omega_l) \qquad (r \rightarrow \infty) \tag{21}$$

The eigenchannel wave functions (20) are energy-normalized in Rydberg units.[20] In general, the sum of eigenphases changes by π when passing through a resonance. If a single eigenphase changes by π, the associated eigenchannel wave function represents a resonant state.[19]

2.2. One-Axis Model. When ionization occurs only through the transition dipole moment along a certain axis in the

TABLE 1: Correlation of Bound State Orbitals[a]

type	benzene D_{6h}	pyrazine D_{2h}	pyrimdine C_{2v}	pyridine C_{2v}	pyrrole C_{2v}	furan C_{2v}
π	X $1e_{1g}(zx)$	C $1b_{2g}$	A $2b_1$	B $2b_1$	A $2b_1$	A $2b_1$
π	X $1e_{1g}(yz)$	A $1b_{1g}$	C $1a_2$	A $1a_2$	X $1a_2$	X $1a_2$
σ	A $3e_{2g}(xy)$	D $3b_{3g}$	X $7b_2(n)$	C $7b_2$		
σ	A $3e_{2g}(x^2-y^2)$	X $6a_g(n)$	B $11a_1(n)$	X $11a_1(n)$		
σ	C $3e_{1u}(x)$	B $5b_{1u}(n)$				
σ	C $3e_{1u}(y)$	F $4b_{2u}$		$6b_2$		

[a] Nonbonding orbitals are indicated by (n). X denotes the ground state of a cation, while A−F are excited states from lower to higher.

molecular frame, the laboratory frame (LF) and molecular frame (MF) PADs are simply related. If the ionization dipole moment is along the molecular z-axis, the following relation holds

$$I_{lm\mu} = I_{lm\mu}\delta_{0\mu} \tag{22}$$

where $\delta_{0\mu}$ is the Kronecker delta. The corresponding MF-PAD is written as

$$\frac{d\sigma(E)}{d\Omega} = \sum_{lm}\beta_{lm}^{MF}(E)\, Y_{lm}(\theta,\phi) \tag{23}$$

Substituting (22) into (4) and comparing that with the MF-PAD formula by Dill,[21] we obtain the asymmetry parameter in the laboratory frame to be

$$\beta(E) = \frac{2}{\sqrt{5}}\frac{\beta_{20}^{MF}(E)}{\beta_{00}^{MF}(E)} \tag{24}$$

The convolution of (23) with the alignment function of a molecule also leads to the same equation (Appendix). The factor $2/\sqrt{5}$ comes from the axis alignment parameter. In (24), the β values are 2 and -1 for $\beta_{20}^{MF}/\beta_{00}^{MF} = \sqrt{5}$ and $-\sqrt{5}/2$, respectively. The $\sqrt{5}$ and $-\sqrt{5}/2$ correspond to unrealistic extreme cases where MF-PAD becomes a δ function. In other words, β never actually reaches the upper ($\beta = 2$) or lower ($\beta = -1$) bound in this one-axis model.

2.3. Details of Calculation. Bound state molecular orbitals were calculated using the GAMESS package[22] by the HF/4-31G method. A parallel CMSXα code was written for continuum wave functions. A muffin-tin potential takes different forms in three spatial regions: Region I denotes the inside of the spheres centered at atomic nucleii. Region II denotes the outside of region I and the inside of a large sphere around the center of mass of a molecule. For region I, we used a touching sphere model, which prevents the overlapping of atomic spheres, with an experimentally determined molecular geometry[14,23−28] and Slater's Xα potential with the parameter $\alpha = 1.0$. The touching sphere model usually employs $\alpha = 1.0$; however, 0.83−0.93 have been found as the optimized values for reproducing experimentally observed σ-type resonances in diatomic molecules.[10] The radii of spheres were determined as follows: (1) Half of the chemical bond length is given to a pair of atoms as the initial atomic radius. (C═C bonds were chosen in the first step for benzene, pyrazine, pyrrole, and furan and C═N bonds for pyridine and pyrimidine.) (2) The radii are adjusted to achieve self-consistency to create contact between spheres. The outside of region II is region III. The potential in region III is a pure Coulomb potential with a unit charge[13] located at the center of mass of a molecule. The resulting parameters are listed in Table S1 (Supporting Information).

For a given photon energy, continuum wave functions are evaluated using K-matrix formalism, utilizing experimental ionization potentials (see Table S2 in the Supporting Information).[2,14,29−35] Then, they are orthogonalized with fully occupied orbitals. Partial wave expansion was truncated at $l_{max} = 5$ (8) in region I and at $l_{max} = 7$ (10) in regions II and III for π (σ and n) ionization. To obtain converged differential cross sections, higher angular momentum partial waves were required for σ and n orbitals than for π orbitals, because the σ and n orbitals considered here have many angular nodes. The contribution of the largest partial waves ($l = l_{max}$) alters $\beta(E)$ by less than 0.1 in ionization of the entire energy range, and especially less than 0.01 for $E < 10$ eV. Therefore, the results are particularly reliable for $E < 10$ eV. Because experimental uncertainty in $\beta(E)$ is $\pm 0.05-0.12$,[2−5] the convergence of theoretical calculation is good enough to compare the calculated $\beta(E)$ with the experimental one. We followed an axis convention by Mulliken.[36]

3. Results and Discussion

3.1. Correlation of Bound and Resonant Orbitals. We considered ionization from orbitals that correlate with the $1e_{1g}(\pi)$, $3e_{2g}(\sigma)$, or $3e_{1u}(\sigma)$ orbitals of benzene. We have confirmed correlation of the orbitals between different molecules from their symmetries and energies. Excluded from our discussion are the pyrimidine $10a_1$ and $6b_2$ orbitals, and the pyridine $11b_2$ orbitals that were found to deviate substantially from the benzene orbitals. The resulting 22 orbitals are summarized in Table 1 and Figure S1 (Supporting Information).

The σ and π orbitals of planar molecules are categorized into the a′ and a″ symmetries in the C_s point group, respectively. For azabenzenes, the bonding orbitals with the a′ symmetry are subdivided into nonbonding (n) orbitals that are mainly localized around the nitrogen atoms and bonding (σ) orbitals that largely constitute the six-membered aromatic ring framework. The pyrazine $6a_g$ and $5b_{1u}$ orbitals, the pyrimidine $7b_2$ and $11a_1$ orbitals, and the pyridine $11a_1$ orbitals are n-orbitals. Note that the π and σ orbitals are not significantly different from their corresponding benzene orbitals, because the nitrogen atoms of these heteroaromatic molecules are located on the nodes of the π and σ electron wave functions.

Continuum wave functions with the a′ and a″ symmetries are denoted as $k\sigma$ and $k\pi$, respectively. The resonance states are indicated by σ^* or π^* . It is useful to examine the resonance energies from the eigenphase sum in evaluating the quality of muffin-tin potentials before performing time-consuming calculations of the transition dipole moments (16). If necessary the model parameters can be adjusted so as to reproduce the known resonance energies. A small difference in α parameters leads to a noticeable difference in shape-resonance energies. CMSXα calculations by Carlson et al. predicted seven σ^* and one π^* (b_{2g}) resonance states for benzene[14] (Table 2). On the other hand, our calculations predict another π^* (b_{1g}) state just above the threshold, in addition to the eight states predicted by Carlson et al.[14] at almost the same positions. For heteroaromatic molecules, there is no signature of the shape resonance with the π^* state. Because π^* (b_{1g}) and π^* (b_{2g}) are inaccessible by

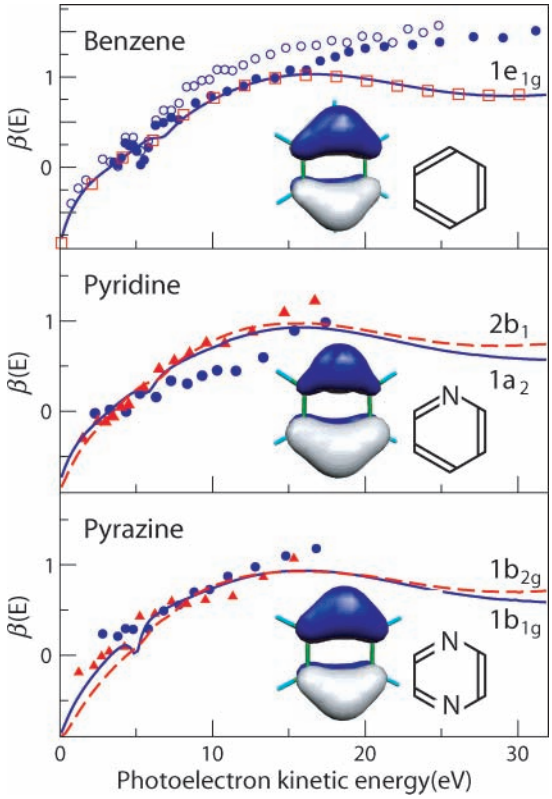

Figure 1. Asymmetry parameters for π electron ionization as functions of excess energy. The highest occupied π orbitals are represented by solid lines for the calculated values and by circles for the observed ones, and the second occupied π orbitals by dashed lines and triangles, respectively. Experimental values are taken from Carlson et al. (1987) (○) and Baltzer (1997) et al. (●) for benzene and from Piancastelli et al. (1983) for pyrazine and pyridine. The size of symbol represents the typical experimental error in β. Larger basis (6-31G*) results are indicated by (square).

TABLE 2: Correlations of σ* Resonant States

type	D_{6h}	D_{2h}	C_{2v}	C_s
1	$e_{1u}(x)$	b_{1u}	a_1	a′
2	$e_{1u}(y)$	b_{2u}	b_2	a′
3	b_{1u}	b_{1u}	a_1	a′
4	$e_{2g}(x^2 - y^2)$	a_g	a_1	a′
5	$e_{2g}(xy)$	b_{3g}	b_2	a′
6	a_{1g}	a_g	a_1	a′
7	a_{2g}	b_{3g}	b_2	a′

dipole transitions from the ionized orbitals considered below, these are unimportant in the present case.

3.2. $1e_{1g}(\pi)$-Type Ionizations. Figures 1 and 2 show the calculated $\beta(E)$ values for benzene, pyridine, pyrazine, pyrimidine, pyrrole, and furan. These values agree rather well with the experimental values, particularly up to ca. $E = 16$ eV, except for the pyridine $1a_2$: the asymmetry parameter experimentally observed for the $1a_2$ band of pyridine seems to increase more slowly than the calculation. However, this should be considered carefully, as it is due at least in part to a signal contamination of the $1a_2$ band with an overlapping $11a_1$ band (nonbonding orbital).[2] Above 16 eV, our β values appear systematically lower than the experimental ones and those obtained by Carlson et al.[14]

We have examined the dependence of calculated $\beta(E)$ on a basis set size by performing calculations at the 6-31G* level for benzene. The muffin-tin potential (V_{II}) calculated at the 6-31G* level was energetically lower than that of 4-31G by $V_{II}^{6-31G^*} - V_{II}^{4-31G} = -0.03$ au on average. However, we found

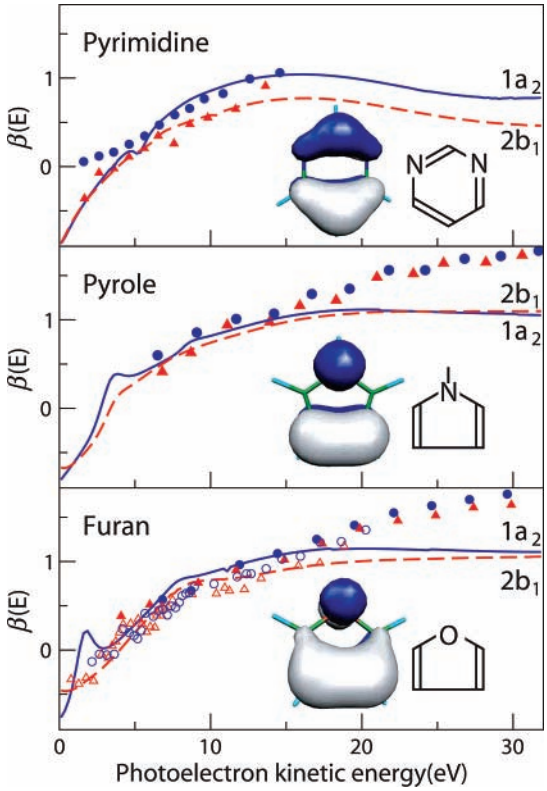

Figure 2. Asymmetry parameters for π electron ionization as functions of excess energy. The highest π orbitals are represented by solid lines for the calculated values and by filled circles for the observed ones, and the second highest π orbitals by dashed lines and filled triangles, respectively. Experimental values are taken from Piancastelli et al. (1983) for pyrimidine and Holland et al. (2001) (filled symbol) and Keller et al. (1984) (open symbol) for pyrrole and furan. The size of symbol represents the typical experimental error in β.

TABLE 3: Low-Energy Parameters for π Ionization $E = 0.1$ eV

		A_0	A_1	A_2	$\Xi_{1,3}$	A_3	A_4
benzene	$1e_{1g}$	−0.38	0	0.53	0.91	0	0.00
pyridine	$1a_2$	−0.34	0.00	0.53	0.89	0.02	0.00
	$2b_1$	−0.34	0.01	0.53	1.03	0.00	0.00
pyrazine	$1b_{1g}$	−0.38	0	0.50	1.02	0	0.00
	$1b_{2g}$	−0.32	0	0.57	1.15	0	0.00
pyrimidine	$2b_1$	−0.34	0.01	0.53	1.10	0.01	0.00
	$1a_2$	−0.34	0.00	0.54	1.05	0.01	0.00
pyrrole	$1a_2$	−0.42	0.00	0.40	1.01	0.00	0.00
	$2b_1$	−0.32	0.01	0.40	1.13	0.01	0.00
furan	$1a_2$	−0.39	0.00	0.37	1.07	0.00	0.00
	$2b_1$	−0.20	0.16	0.32	1.16	0.02	0.00

that the 6-31G* muffin-tin potential provides the same $\beta(E)$ with the 4-31G case (Figure 1), suggesting that calculations are converged for the basis set size.

A sharp increase of $\beta(E)$ in the low-energy region is a common feature of all π orbitals of heteroaromatic molecules. A similar feature was previously observed in ionization from the π orbitals of small molecules,[2−5] which was ascribed by Thiel to the energy-dependent Coulomb phase.[10] To examine the Coulomb phase effect in the present case, we performed a model calculation in which $\beta(E)$ is extrapolated for different energies considering only the energy dependence of the Coulomb phase with a constant $I_{lm\mu}(E)$, at $E = 0.1$ eV. Figure 3a shows the thus-predicted asymmetry parameters (solid line). The result shows that this simple model captures the uprising features of $\beta(E)$, supporting the notion presented by Thiel.

Although the importance of the Coulomb phase is quite apparent, the experimental and calculated $\beta(E)$ for π orbitals

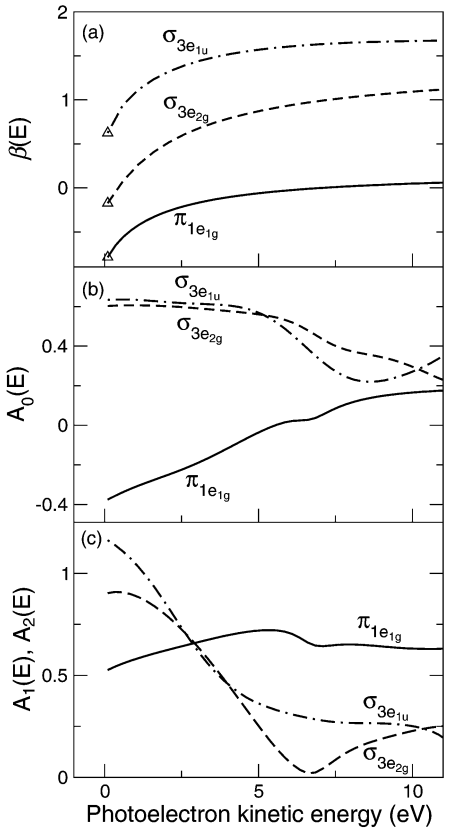

Figure 3. (a) Asymmetry parameter by model calculations, where transition dipole moments are fixed at $E = 0.1$ (marked with triangles), (b) $A_0(E)$ for the benzene orbitals, and (c) $A_1(E)$ for the $3e_{1u}$ orbital and $A_2(E)$ for the $3e_{2g}$ and $1e_{1g}$ orbitals of benzene.

(Figure 1) increase more rapidly than $\beta(E)$ of the model (Figure 3a). As discussed for (5), $\beta(E)$ can be expressed by the parameters $A_l(E)$ and $\Xi_{l-l+}(E)$. $A_0(E)$ and $A_2(E)$ for benzene are shown in Figure 3b,c (solid lines). Those parameters near the ionization threshold have some common features: in ionization from the π orbitals of benzene and the heteroaromatics, $A_0(E)$ is negative near the threshold (Table 3). A_1 is strictly zero for benzene and pyrazine for symmetry reasons, and it is nonzero but small for other molecules. A major interference term arises from A_2. Further higher angular momentum partial waves contribute less than 4% at $E < 5$ eV for benzene $1e_{1g}$, due to a centrifugal barrier. An approximate formula for the asymmetry parameter is, hence, obtained as

$$\beta(E) \approx A_0 - A_2 \cos(\eta_1(E) - \eta_3(E) + \Xi_{1,3}\pi) \qquad (25)$$

where A_2 is positive and $\Xi_{1,3} \approx 0.9-1.2$ (Table 3). Although eq 8 for $\Xi_{1,3}(E)$ is complicated, the common feature of $\beta(E)$ suggests that there is a notable similarity between $\Xi_{1,3}(E)$ in different systems. Because the ionized orbitals have similar shapes, the similarity of $\beta(E)$ imply the corresponding continuum wave functions resemble to each other between different systems.

Equation 25 is analogous to the Cooper−Zare formula for atomic nd → *k*p,*k*f ionization, where A_0 is positive and $\Xi_{1,3}(0) = 0.5$ for Kr and Xe[37] with a weak energy dependence. The atomic $\Xi_{1,3}(E)$ is related to the difference in quantum defects as $\lim_{E\to 0}\Xi_{1,3}(E) = \delta_p - \delta_f$.[38] Although the interpretation of the molecular $\Xi_{l-l+}(E)$ is not as simple as that in atomic cases, $\Xi_{1,3}(E)$ is found to be almost invariant with energy in ionization from π orbitals.

Because $A_2(E)$ and $\Xi_{1,3}(E)$ do not vary rapidly in the low-energy region, the negative and uprising $A_0(E)$ (Figure 3b, solid line) is the second origin of the rapid increase of $\beta(E)$ for π orbitals. Then, why does $A_0(E)$ start from a negative value and increases with energy? The π orbitals considered in this study are approximated by an atomic 3d orbital, in a united atom picture, as shown in Figure 1, 2, or S1 (Supporting Information): for instance, the benzene $1e_{1g}(zx)$ orbital is similar to $3d_{zx}$. The *k*p and *k*f continua are reached by dipole transition from an atomic d orbital. We can treat those two continua separately, because $A_0(E)$ of eqs 9 and 13 does not have any interference term between *k*p and *k*f.

First, we consider the *k*p continuum. There are two components, kp_x and kp_z, which can be accessed by the dipole transition with polarization along *z* and *x* axis, respectively. In either case, $\sin^2(\theta_k)$ distribution and negative $A_0(E)$ are observed. CMSXα calculation shows that the parital cross section for kp_z is more than 6 times smaller than for kp_x at $E = 0.1$ eV; i.e., the photoelectron is more ejected in the molecular plane than in perpendicular direction to it. If we neglect the small contribution of ionization into kp_z continuum, we are able to apply one-axis model to evaluate $A_0(E)$

$$A_0(E) = \frac{2}{\sqrt{5}} \times \frac{-1}{\sqrt{5}} = -0.4 \qquad (26)$$

where $-1/\sqrt{5}$ is the molecular frame anisotropy parameter, $\beta_{20}^{MF}/\beta_{00}^{MF}$, for the photoelectron angular distribution $d\sigma/d\Omega \propto \sin^2(\tilde{\theta}_k)\cos^2(\tilde{\phi}_k)$. When the contribution of kp_z increases for higher excess energy, both kp_x and kp_z channels must be taken into account. Their interference effect can give rise to a positive $A_0(E)$. For instance, the $A_0(E)$ is 0.2 for spherical potential, which can be derived from the Cooper−Zare formula:[1]

$$A_0(E) = \frac{(l-1)}{2l+1} = 0.2 \qquad (27)$$

where only the ionization from $d(l=2)$ to *k*p is assumed.

We have found that the ionization into the *k*f continuum also provides negative contribution to $A_0(E)$ near threshold and positive contribution at $E > 4$ eV, though the angular distributions of the component of the *k*f continuum wave functions have complicated structure.

Ionization from the $1e_{1g}$ orbital of benzene exhibits a small dip in $\beta(E)$ due to shape resonance at $E = 5$ eV (Figure 1). The appearance of shape resonance in $\beta(E)$ has been observed for ionization from the π orbitals of small molecules.[4] For benzene, because we take into account partial waves of up to $l_{max} = 7$, seven $e_{1u}(x)$ eigenchannels exist. To identify which of these is in resonance, we examined the eigenphases of ke_{1u} continuum wave functions shown in Figure 4. One of the eigenchannels exhibits a rapid change in phase at approximately 5 eV, indicating that this channel is solely responsible for the shape resonance. Figure 5 shows this particular eigenchannel wave function $\xi_\gamma(r,\theta,\phi,k)$ of benzene $k\sigma^*e_{1u}(x)$ continuum in the (a) off-resonance and (b) on-resonance. The maximum amplitude of this wave function in the molecular plane is approximately $|\xi_\gamma| = 0.14$ au at 4.9 eV and reaches 0.68 au on resonance. The effects of the $k\sigma^*e_{1u}(x)$ shape resonance on $\beta(E)$ and the integral cross section are rather weak, because the transition dipole from the π orbital to the σ^* orbital is small. Also note that the interference term (Δl, $\Delta m = 0, \pm 1, \pm 2$) in eq 2 is expected to be small in this case, because the background states consist of $m = 0$ and 1, whereas the resonance state is of $m = 5$, as seen in Figure 5a. The cross terms of m and m' have to share the

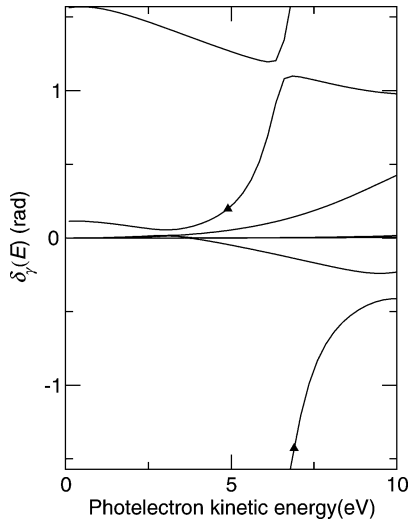

Figure 4. $k\mathrm{e}_{1u}$ eigenphase of benzene. Seven e_{1u} channels exist under the condition of $l_{max} = 7$, but three of them are constantly close to zero. The solid triangle represent the points referred to in the Figure 5.

same m_t due to Clebsch−Gordan coefficients, $(1-\mu\ lm|j_t m_t)$ and $(1-\mu'\ l'm'|j_t m_t)$ of eq. 2, while m_t differs by μ and μ' from m and m', respectively. Hence, the $|m-m'|$ of non zero terms are equal to $|\mu-\mu'| \leq 2$. Because the maximum amplitude of the σ^* wave function is in the molecular plane, $\pi \rightarrow \sigma^*$ resonance provides electrons ejected perpendicular to the light polarization and reduces $\beta(E)$. For heteroaromatic molecules, such singularities are seen for orbitals correlated with $1\mathrm{e}_{1g}(yz)$, i.e., $1\mathrm{b}_{1g}$ of pyrazine and $1\mathrm{a}_2$ of C_{2v} molecules (Figures 1 and 2). As will be discussed in the next section, the $k\mathrm{b}_{1u}$ (**1**) resonance state of pyrazine has a large contribution from a single eigenchannel. The shape of the wave function is presented in Figure 5c. In contrast, the dips are almost invisible in ionization from orbitals correlated with benzene $1\mathrm{e}_{1g}(xz)$.

3.3. $3\mathrm{e}_{2g}(\sigma,n)$-Type Ionizations. The upper panels of Figure 6a−d show asymmetry parameters in the $3\mathrm{e}_{2g}(\sigma)$ ionization of benzene and similar ionization processes in azabenzene. These curves exhibit common features of $\beta(E)$ varying in the narrow range of $-0.33 \leq \beta \leq 1.0$ (calculations) and $-0.25 \leq \beta \leq 0.5$ (experiments), regardless of the orbital character (σ or n). Features due to shape resonance are similar, although the resonance energy shifts in the order pyrazine ∼ pyrimidine < pyridine < benzene. Only three resonance states of **1**, **2**, and **3** in Table 2 are symmetry-allowed for benzene and pyrazine, whereas all six states are possible for molecules with the C_{2v} symmetry. A number of resonances cause an irregular variation in $\beta(E)$ in ionization from pyrimidine $7\mathrm{b}_2$. $\beta(E)$ values near the threshold are quite similar between benzene and heteroaromatics. The calculated β is somewhat larger than the observed β. It is noted that the vibrational motion of a molecule is completely neglected in the calculation, and the resonance energy, peak-height and $\beta(E)$ will vary with nuclear displacements, which might reduce the calculated energy dependence of $\beta(E)$. On the other hand, the kinetic energy resolution in experiments was in the range of 50 meV to 0.2 eV,[2−5] and $\beta(E)$ was averaged over kinetic energies with a typical bandwidth of 0.5 eV (fwhm).[2−5] Such averaging may flatten the structure in observed $\beta(E)$.

The energy dependence of $\beta(E)$ up to $E \approx 2$ eV is explained by the Coulomb phase (Figure 3a). The relevant parameters for eq 25 are listed in Table 4. Above 2 eV, one important difference from π ionization is rapidly decreasing $A_2(E)$ (Figure 3c, dashed line). This change masks the energy variation of the Coulomb phase. The decrease of $A_2(E)$ can be understood from eq 15

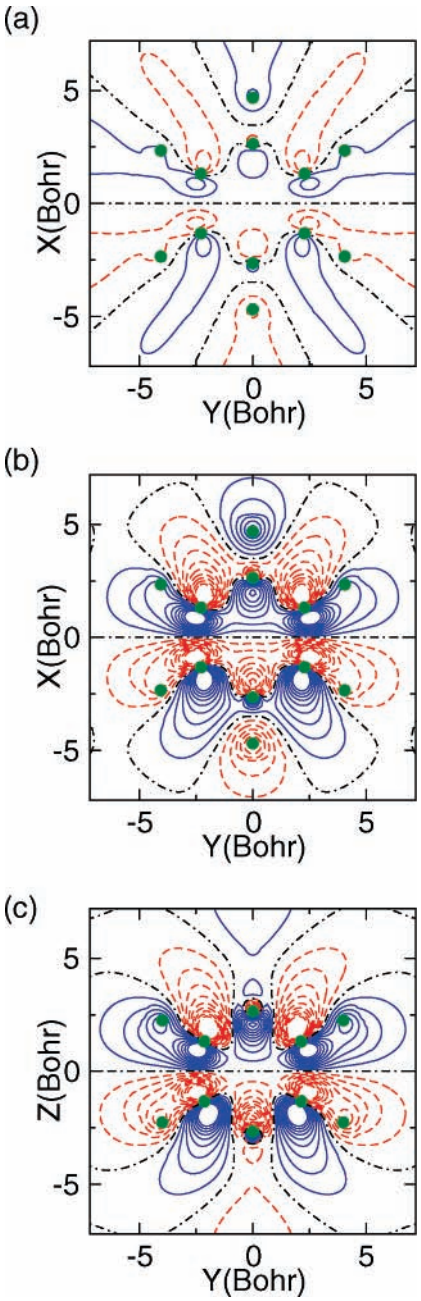

Figure 5. $k\mathrm{e}_{1u}$ eigenchannel wave functions in molecular plane ($Z = 0$) for benzene (a, b) and eigenchannel wave function of resonant $k\mathrm{b}_{1u}$ state for pyrazine (c). The photonelectron kinetic energies are (a) 4.9 eV (off resonance), (b) 6.9 eV (on resonance), and (c) 5.7 eV. The ranges of contours are (a) ± 0.10, (b) ±0.45, and (c) ±0.45 with 0.05 spacings. Solid, dashed, and dot-dashed lines represent positive, negative, and zero values, respectively. Green points represent atomic positions.

and the shape resonance of **1** or **2** at $E \approx 7$ eV, whose wave function dominantly consists of $l = 5$ (Figure 5b). In this situation, the ionization into both kp and kf continuum becomes negligible, and hence $A_2(E)$ approaches zero, due to eq 15.

In the $3\mathrm{e}_{2g}$-type ionization, $k\sigma$ channels (Figure 6) are accessible via two axes in the molecular plane. As shown in Table 5, when the partial cross section of one axis exceeds 80% of the integral cross section, eqs 3 and 24 can predict $\beta(E)$ within an error of ±0.2. The peak of $\beta(E)$ slightly shifts in energy from the resonance position as a result of the interference between resonance-mediated ionization and direct ionization.

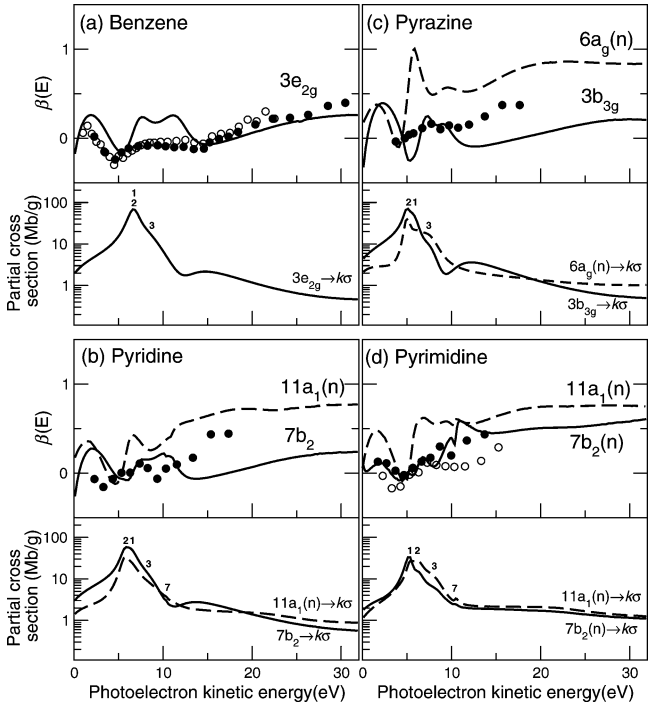

Figure 6. Asymmetry parameters and partial cross sections as functions of photoelectron kinetic energy for benzene $3e_{2g}(xy)$, and corresponding orbitals of pyrazine, pyridine, and pyrimidine (solid lines), and corresponding orbitals of benzene $3e_{2g}(x^2 - y^2)$ (dashed line) [upper panels]. Experimental values are cited from Carlson et al. (1987) (○) and Baltzer (1997) et al. (●) for benzene and from Piancastelli et al. (1983) for pyrazine $6a_g$ (●), pyridine $11a_1$ (●), and pyrimidine $11a_1$ (●) and $7b_2$ (○). The size of symbol represents the typical experimental error in β. Partial channel cross section (σ,n → $k\sigma$) was divided by degeneracy, $g = 4$ for e_{2g}, $g = 2$ for the other orbitals [lower panels]. The numbers indicate the resonant states listed in Table 2.

We may examine the validity of one-axis approximation from the ratio of the partial cross section for ionization via a certain axis to the total, ρ (% in Table 5). An experimental assessment of the one-axis model is possible through the measurement of photoionization probability for aligned ensemble of molecules. For these experiments, we previously defined $b_{KLk_\gamma\Lambda p}$ coefficients,[39] by which ρ can be written as

$$\rho = \begin{cases} \frac{1}{3} + 5\dfrac{b_{20200} - \sqrt{3}b_{20220}}{3\sqrt{10}b_{00000}}, & X \\ \frac{1}{3} + 5\dfrac{b_{20200} + \sqrt{3}b_{20220}}{3\sqrt{10}b_{00000}}, & Y \\ \frac{1}{3} - \dfrac{\sqrt{10}}{3}\dfrac{b_{202000}}{b_{00000}}, & Z \end{cases} \tag{28}$$

where X, Y, and Z denote the axis of ionization in the molecular frame. The $b_{KLk_\gamma\Lambda p}$ coefficient can be observed by time-resolved photoelectron spectroscopy[40] or IR + VUV two-photon ionization spectroscopy,[41] where the first infrared light creates the aligned neutral molecules in the vibrationally excited state. There are also calculations of ρ but in different form. Wallace and Dill[42] defined the same value by another parameter as

$$\rho = \frac{1 + \beta_{\hat{n}}}{3} \tag{29}$$

where the $\beta_{\hat{n}}$ varies from −1 to 2, whereas ρ changes from 0 to 1 correspondingly. Lucchese et al. have found that $\beta_{\hat{n}}$ reaches

TABLE 4: Major A_l and Ξ_{l-l_+} Values at $E = 0.1$ eV for Benzene $3e_{2g}$ and Related Ionizations

	orbital	A_0	A_2	$\Xi_{1,3}$
σ				
	benzene $3e_{2g}$	0.60	0.90	1.00
	pyridine $7b_2$	0.50	0.91	0.98
	pyrazine $3b_{3g}$	0.44	0.95	0.95
n				
	pyridine $11a_1$	0.76	0.56	1.11
	pyrazine $6a_g$	0.86	0.72	1.07
	pyrimidine $7b_2$	0.63	0.64	1.24
	pyrimidine $11a_1$	0.68	0.65	1.00

TABLE 5: One-Axis Approximation near Resonance Energies in σ Ionization

	ϕ_0	E (eV)	axis[a]	%	type[b]	Γ [c]	$2\beta_{20}^{MF}/\sqrt{5}\beta_{00}^{MF}$	β[d]
pyrazine	$6a_g$	4.85	Y	92	2	b_{2u}	0.21	0.29
		7.35	Z	82	3	b_{1u}	0.38	0.53
	$3b_{3g}$	6.1	Y	89	1	b_{1u}	−0.12	−0.13
		4.85	Z	52	2	b_{2u}	0.35	−0.16
	$5b_{1u}$	3.85[e]	Z	28	4	a_g	0.06	0.51
		4.1	Y	67	5	b_{3g}	0.27	0.46
		10.1	Y	49	7	b_{3g}	0.15	0.11
	$4b_{2u}$	3.85[e]	Z	42	5	b_{3g}	−0.17	0.17
		6.6	Y	84	6	a_g	0.35	0.15
		10.1	Z	67	7	b_{3g}	0.65	0.36
pyrimidine	$11a_1$	5.1	Z	93	1	a_1	−0.19	−0.08
		8.1	Z	57	3	a_1	0.35	0.55
	$7b_2$	5.35	Y	72	1	a_1	−0.04	−0.01
		10.6[e]	Z	36	6	b_2	0.23	0.51
pyridine	$11a_1$	5.6	Y	79	2	b_2	0.20	0.09
		7.85	Z	73	3	a_1	0.24	0.30
	$7b_2$	3.1	Y	76	1[f]	a_1	−0.04	0.20
		5.6	Z	53	2	b_2	0.43	−0.07
		7.85	Y	82	1	a_1	0.14	0.15
	$6b_2$	4.60[e]	Z	25	5	b_2	−0.05	0.45
		8.10	Y	83	6	a_1	0.38	0.26
		10.85	Z	49	7	b_2	0.53	0.36

[a] Molecular axis with largest cross section. [b] Type of resonance state in Table 2. [c] Symmetry of continuum wave function, which satisfies $\Gamma_{\phi 0} \otimes \Gamma_{axis} \oplus \Gamma_k \ni \Gamma_A$. [d] Present CMSXα calculation. [e] Peak position of partial cross section. [f] At low-energy side of resonance **1**.

2 in a photoionization of N_2 molecules by the Schwinger variational method,[43] where a one-axis model is certainly applicable.

In section 2.2, we have mentioned that when the one-axis approximation is applicable, $\beta(E)$ hardly reaches the limiting values, −1 or 2. Even so, the values listed in Table 5 are remarkably close to zero (−0.19-0.65). This can be understood from the shape of $k\sigma^*$ resonant wave functions. The ionization from σ to $k\sigma^*$ is only allowed via the transition dipole that is in the molecular plane. Then, the photoelectrons are ejected in the molecular plane but not specifically to parallel or perpendicular direction to the dipole, because the $k\sigma^*$ wave functions do not have specific direction in the molecular plane as illustrated in Figure 5b,c. Those rather isotropic wave functions result in the $\beta(E) \approx 0$.

It is difficult to distinguish between σ and n orbitals by $\beta(E)$, especially between $E = 2$ and 15 eV. However, the maximum of the partial cross section at $E \approx 5$ eV is smaller for n → $k\sigma$ than for σ → $k\sigma$ (Figure 6). This difference arises from the shapes of wave functions. As an example, a resonant eigenchannel wave function of pyrazine $k b_{1u}[\sigma^*(\mathbf{1})]$ is shown in Figure 5c. There is a difference between the benzene $k e_{1u}(x)$ orbital and the pyrazine $k b_{1u}$ orbital in that the C−H* character is lacking in the latter, which reduces the transition dipole moment for n → $\sigma^*(\mathbf{1})$ ionization.

3.4. $3e_{1u}(\sigma,n)$-Type Ionizations. $\beta(E)$ values in ionization from benzene $3e_{1u}$ and related orbitals exhibit similar features

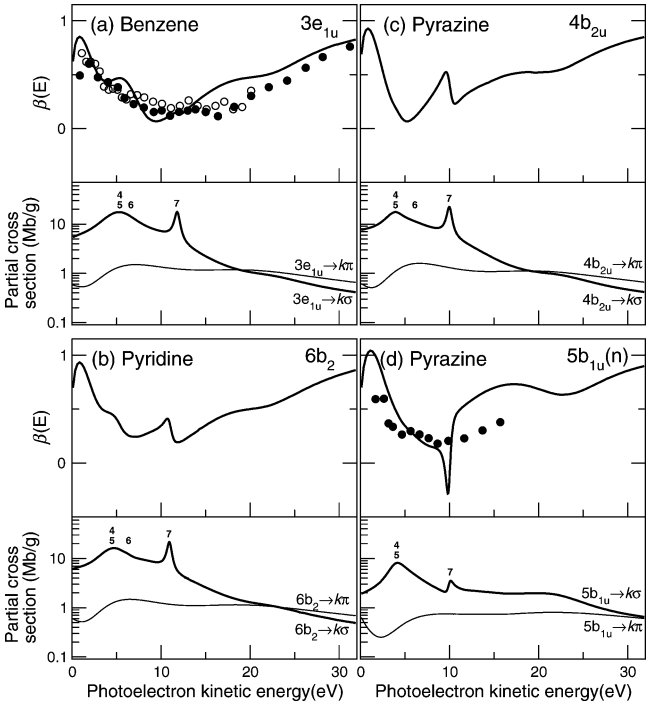

Figure 7. Asymmetry parameters as functions of photon energy for (a) benzene $3e_{1u}$, and corresponding orbitals of (b) pyridine and (c, d) pyrazine [upper panels]. Experimental values are cited from Carlson et al. (1987) (○) and Baltzer et al. (1997) (●) for benzene and from Piancastelli et al. (1983) for pyrazine (●). The size of symbol represents the typical experimental error in β. Partial channel cross section divided by degeneracy: $g = 4$ for e_{1u} and $g = 2$ for the other orbitals [lower panels]. Bold lines indicate the σ and n ionizations to the $k\sigma$ channel. Thin lines indicate the ionization to the $k\pi$ channel. The numbers indicate the resonant states in Table 2.

TABLE 6: Major A_l and Ξ_{l-l_+} Values at $E = 0.1$ eV for Benzene $3e_{1u}$ and Related Ionizations

	orbital	A_0	A_1	$\Xi_{0,2}$
σ				
	benzene $3e_{1u}$	0.63	1.16	0.59
	pyridine $6b_2$	0.64	1.17	0.58
	pyrazine $4b_{2u}$	0.65	1.15	0.58
n				
	pyrazine $5b_{1u}$	0.64	1.00	0.57

(upper panels of Figure 7a−d). They exhibit their maxima near the threshold and their minima at approximately $E = 10$ eV, and gradually increase beyond. In contrast to those of the previous two types of orbital, $\beta(E)$ is always positive in the entire range, except for the value for ionization from the pyrazine $5b_{1u}$ orbital at $E = 10$ eV. Peak positions in the calculated $\beta(E)$ curves are shifted lower in the order of pyrazine $4b_{2u}$ < pyridine $6b_2$ < benzene $3e_{1u}$, reflecting their resonance energies.

Figure 3a (dot-dashed line) shows that the Coulomb phase primarily controls the energy variation of $\beta(E)$ only near the threshold ($E < 1$ eV) with the following formula:

$$\beta(E) \approx A_0 + A_1 \sin(\eta_0(E) - \eta_2(E)) \qquad (30)$$

where the parameters are listed in Table 6. A_0 is close to the value for $3e_{2g}$-type ionization (Table 6). The difference in $\beta(E)$ from $3e_{2g}$-type ionization arises from the phase shift $\Xi_{0,2} \approx 0.5$, from which the sine form of eq 30 is obtained. The energy variation of $A_1(E)$ is far larger than that of the Coulomb phase at higher energy $E > 2$ eV (Figure 3c, dot-dashed line). The decreasing $A_l(E)$ is caused by the relative reduction of the ks and kd partial cross sections to the total, through the eq 15. The partial cross secition of ks and kd is more than 95% at the ionization threshold but ca. 30% at $E \approx 7$ eV, because the wave functions of the lowest resonance states (**4** or **5**) have mainly high orbital angular momentum of $l = 4$. Table 6 shows a little difference between the σ and n orbitals, where the partial cross section of n → $k\sigma$ ionization is 3−4 times smaller than that of $\sigma \rightarrow k\sigma$ ionization (Figure 7) at $E = 0.1$ eV, due to a small transition dipole from the n state to the broad σ^*(**6**, C−H*) resonant state.

Above 10 eV, the calculated $\beta(E)$ of the n orbital (pyrazine $5b_{1u}$) is higher than those of the other orbitals. However, the corresponding experimental results are rather few. Only $\beta(E)$ observed for pyrazine $5b_{1u}$ seems greater than the value for benzene $3e_{1u}$ at 14−15 eV.

σ and n ionizations show a difference in partial cross sections in the region of 25−32 eV where σ orbitals ionize more to the $k\pi$ channel than to the $k\sigma$ channel (Figure 7), which is consistent with the results for benzene ($3e_{1u}$) obtained by Wilhelmy et al.[44] and Venuti et al.[45] In contrast, the $k\sigma$ channel is calculated to be more favored in n ionization for the entire energy range. This difference between σ and n in the partial cross sections is also observed for $3e_{2g}$-type ionization in the same energy region (not shown).

On the basis of the partial cross sections, we conclude that there are clearly n-subgroups for $3e_{1u}$-type ionizations as well as $3e_{2g}$-type ionizations. The missing n → σ^* (C−H*) ionization is the origin for the deviation of n from σ in the partial cross section near the threshold.

4. Conclusion

We have calculated asymmetry parameters as functions of photoelectron kinetic energy for ionization from various orbitals of heteroaromatic molecules. The calculations have well reproduced observed $\beta(E)$, especially between $E = 0$ and 16 eV. Between 0 and 1 eV, $\beta(E)$ for all orbitals but pyrimidine $7b_2$ show increases, which has been explained by the energy variation of the Coulomb phase. The energy variation of the Coulomb phase affects $\beta(E)$ through the interference terms of $A_l(E)$, $l \geq 1$ of eq 7, and the relevant interference term is $A_1(E)$ or $A_2(E)$ at 0.1 eV, due to the centrifugal barrier. Above 1 eV, $\beta(E)$ for π orbitals increase more rapidly than anticipated by this simple model. This difference is ascribed to the behavior of $A_0(E)$ that is negative near the threshold, analogously with atomic $3d_{xz} \rightarrow kp_x$ single channel ionization via the transition dipole along the z axis, and then becomes positive for $E > 5$ eV as a result of interference between the kp_x and kp_z scattering wave functions. In ionization from σ and n orbitals above 2 eV, the simple model is completely disrupted by the shape resonances. This disruption is understood by the behavior of $A_1(E)$ and $A_2(E)$. These $A_l(E)$ terms for σ and n almost vanish when the energy approaches the lowest resonant state of **1**, **2**, **4**, or **5** around 5−7 eV, because the resonance enhances the contribution of a certain higher angular momentum outgoing wave and suppress those of the waves $l \leq 3$. Because the wave functions for resonant states, including **3**, **6**, and **7**, are undirected in the molecular plane, and the transition dipole is parallel to the molecular plane, $\beta(E)$ is close to zero for $E \leq 10$ eV, where these resonant states are the dominant ionization channels. Although $A_3(E)$ or $A_4(E)$ appears where two resonant states with different angular momenta are relevant, these terms and $A_0(E)$ cancel out each other to make $\beta(E)$ nearly zero.

Keller et al.[3] discriminated various orbital types, including π, σ, and n orbitals, on the basis of the difference in $\beta(E)$ between photoelectron energies 2 and 10 eV. The selected

energies were rather arbitrary. The near threshold behavior of $\beta(E)$ (Tables 3, 4, and 6) would be an alternative measure for distinguishing the orbital types. For instance, the $\beta(E)$ near threshold ($E \approx 1$ eV) is different among $1e_{1g}$, $3e_{1u}$, and $3e_{2g}$ types of orbital in the present calculation, and in the experiment for π and n orbitals of heteroaromatic molecules. This can be further examined by measurement of $\beta(E)$ for the corresponding σ orbitals of azabenzene. Although there is little difference between σ and n in $\beta(E)$, the partial cross sections of $k\sigma$ continuum are different between them. The partial cross section has never been observed for gas phase molecules; however, the $\beta_{\tilde{n}}(E)$ or the ratio of the $k\sigma$ partial cross section to the total can be observed by time-resolved photoelectron spectroscopy[40] or infrared−VUV photoionization spectroscopy from a single J level.[41] The total cross section should also reflect the difference at resonance, because resonant ionizations into $k\sigma$ continuum dominate the total.

Acknowledgment. This work was supported by a Grant-in-Aid (17205004 and 15002011) from the Ministry of Education, Culture, Sports, Science and Technology. Y.S. thanks the special postdoctoral researcher program at RIKEN. We thank the RIKEN advanced center for computing and communication for allowing us to use the RIKEN Super Combined Cluster.

Appendix: Derivation of Equation 24

In one-axis approximation, doubly differential cross sections are written as

$$\frac{d\sigma}{d\Omega\, d\Omega_M} = \rho(\Omega_M) \sum_{lm} \beta_{lm}^{MF} Y_{lm}(\theta,\phi) \tag{31}$$

where Ω_M is the Euler angle of molecular orientation with respect to the laboratory frame and ρ is the distribution function. $\rho(\Omega_M)$ can be expanded in terms the rotational matrix[46] as

$$\rho(\Omega_M) = \sum_{LMK} d_{LMK} D_{MK}^{L*}(\Omega_M) \tag{32}$$

MF spherical harmonics are transformed by the rotational matrices into the laboratory frame

$$Y_{lm}(\tilde{\theta}_k,\tilde{\phi}_k) = \sum_{m'} Y_{lm'}(\theta_k,\phi_k)\, D_{m'm}^{l}(\Omega_M) \tag{33}$$

Substituting (32) and (33) into (31) and integrating over Ω_M, we obtain

$$\frac{d\sigma}{d\Omega} = \sum_{lmm'} \beta_{lm}^{MF} d_{lm'm} Y_{lm'}(\theta_k,\phi_k)/(2l+1) \tag{34}$$

By parallel ionization, residual ions distribute in the squared cosine form

$$\rho(\Omega_M) = N\{D_{00}^{2*}(\Omega_M) + 2D_{00}^{2*}(\Omega_M)\} \tag{35}$$

$$= \frac{3}{2} N \cos^2 \theta_M \tag{36}$$

where $N = \sqrt{8\pi^2}$ is the normalization factor of $\rho(\Omega_M)$. We can see that $d_{000} = N$ and $d_{200} = 2N$; thus,

$$\frac{d\sigma}{d\Omega} = N\left\{\beta_{00}^{MF} Y_{00}(\theta_k,\phi_k) + \frac{2}{5}\beta_{20}^{MF} Y_{20}(\theta_k,\phi_k)\right\} \tag{37}$$

$$= N\left\{\beta_{00}^{MF}\sqrt{\frac{1}{4\pi}} + \frac{2}{5}\beta_{20}^{MF}\sqrt{\frac{5}{4\pi}} P_2(\cos\theta_k)\right\} \tag{38}$$

From the last equation, $\beta = \beta_{20}^{MF}/\beta_{00}^{MF} \times 2/\sqrt{5}$.

Supporting Information Available: Table S1 containing ionization potentials used for calculations. Table S2 lists the muffin-tin radius and constant potential V_{II}. Figure S1 shows HF/4-31G molecular orbitals. This material is available free of charge via the Internet at http://pubs.acs.org.

References and Notes

(1) (a) Cooper, J.; Zare, R. N. *J. Chem. Phys.* **1968**, *48*, 942. (b) Cooper, J.; Zare, R. N. Photoelectron angular distribution. In *Lectures in theoretical physics*; Gordon and Breach: New York, 1968; Vol. 11c, p 317.
(2) Piancastelli, M.; Keller, P. R.; Taylor, J.; Grimm, F.; Carlson, T. A. *J. Am. Chem. Soc.* **1983**, *105*, 4235.
(3) Keller, P.; Taylor, J.; Grimm, F.; Carlson, T. *Chem. Phys.* **1984**, *90*, 147.
(4) Keller, P.; Taylor, J.; Carlson, T.; Grimm, F. *J. Electron. Spectrosc. Relat. Phenom.* **1984**, *33*, 333.
(5) Holland, D.; Karlsson, L.; von Niessen., W. *J. Electron. Spectrosc. Relat. Phenom.* **2001**, *113*, 221.
(6) Potts, A.; Holland, D.; Trofimov, A.; Schrimer, J.; Karlsson, L.; Siegbahn, K. *J. Phys. B, At. Mol. Opt. Phys.* **2003**, *36*, 3129.
(7) Trofimov, A.; Schirmer, J.; Kobychev, V.; Potts, A.; Holland, D.; Karlsson, L. *J. Phys. B, At. Mol. Opt. Phys.* **2006**, *39*, 305.
(8) Burke, P. G., Berrington K. A., Eds. *Atomic and Molecular Processes: An R-Matrix Approach*; Institute of Physics: Bristol, U.K., 1993.
(9) Lucchese, R. R.; Takatsuka, K.; McKoy, V. *Phys. Rep.* **1985**, *131*, 147.
(10) Thiel, W. *Chem. Phys.* **1983**, *77*, 103.
(11) Kreile, J.; Kurland, H.-D.; Seibel, W.; Schweig, A. *Chem. Phys.* **1991**, *155*, 99.
(12) Grimm, F. A.; Carlson, T. A.; Dress, W. B.; Agron, P.; Thomson, J. O.; Davenport, J. W. *J. Chem. Phys.* **1980**, *72*, 3041.
(13) Thiel, W. *Chem. Phys.* **1981**, *57*, 227.
(14) Carlson, T.; Gerard, P.; Krause, M. O.; Grimm, F.; Pullen, B. *J. Chem. Phys.* **1987**, *86*, 6918.
(15) Dill, D.; Dehmer, J. L. *J. Chem. Phys.* **1974**, *61*, 692.
(16) Abramowitz, M.; Stegun, I. A. *Handbook of Mathematical Functions*, 9th ed.; Dover: New York, 1970.
(17) Dill D.; Fano U. *Phys. Rev. Lett.* **1972**, *29*, 1203.
(18) Chandra N. *Phys. Rev. A* **1987**, *36*, 3163.
(19) Loomba, D.; Wallace, S.; Dill, D.; Dehmer, J. *J. Chem. Phys.* **1981**, *75*, 4546.
(20) Greene, C.; Jungen, C. *Adv. At. Mol. Phys.* **1985**, *21*, 51.
(21) Dill, D. *J. Chem. Phys.* **1976**, *65*, 1130.
(22) Schmidt, M. W.; Baldridge, K. K.; Boatz, J. A.; Elbert, S. T.; Gordon, M. S.; Jensen, J. H.; Koseki, S.; Matsunaga, N.; Nguyen, K. A.; Su, S. J.; Windus, T. L.; Dupis, M.; Motogomery, J. A. *J. Comput. Chem.* **1993**, *14*, 1347.
(23) Mata, F.; Quintana, M. J.; Sorensen, G. O. *J. Mol. Struct.* **1977**, *42*, 1.
(24) Bormans, B. M.; With, G. D.; Mijhoff, F. *J. Mol. Struct.* **1977**, *42*, 121.
(25) Cradock, S.; Liescheski, P. B.; Rankin, D. W. H.; Robertson, H. E. *J. Am. Chem. Soc.* **1988**, *110*, 2758.
(26) Nygaard, L.; Nielsen, J.; Kircheimer, J.; Maltesen, G.; Rastrup-Andersen, N.; Sorensen, G. *J. Mol. Struct.* **1969**, *3*, 491.
(27) Bak, B.; Christensen, D.; Dixon, W.; Hansen-Nygaard, L.; Andersen, J.; Schottlander, M. *J. Mol. Spectrosc.* **1962**, *9*, 124.
(28) Mata, F.; Martin, M.; Sorensen, G. *J. Mol. Struct.* **1978**, *48*, 157.
(29) Reineck, I.; Maripuu, R.; Veenhuizen, H.; Karlsson, L.; Siegbahn, K. M. S. P.; Zu, W. N.; Rong, J. M.; Al-Shamma, S. H. *J. Electron. Spectrosc. Relat. Phenom.* **1982**, *27*, 15.
(30) Yencha, AJ.; El-Sayed, MA. *J. Chem. Phys.* **1968**, *48*, 3469.
(31) Ridley, T.; Lawley, K. P.; Al-Kahali, M. H.; Donovan, R. J. *Chem. Phys. Lett.* **2004**, *390*, 376.
(32) Rennie, E.; Cooper, L.; Johnson, C.; Parker, J.; Mackie, R.; Shpinkova, L.; Holland, D.; Shaw, D.; Hayes, M. *Chem. Phys.* **2001**, *263*, 149.
(33) Derrick, P.; Åsbrink, L.; Edqvist, O.; Jonsson, B. Ö.; Linholm, E. *Int. J. Mass Spectrom. Ion Phys.* **1971**, *6*, 161.
(34) Niessen, M. V.; Cederbaum, L. S.; Diercksen, G. H. F. *J. Chem. Soc.* **1976**, *98*, 2066.

(35) Asbrink, L.; Fridh, C.; Lindholm, E. *J. Eelectron. Spectrosc. Relat. Phenom.* **1979**, *16*, 65.
(36) Mulliken, R. S. *J. Chem. Phys.* **1955**, *23*, 1977.
(37) Kennedy, D. J.; Manson, S. T. *Phys. Rev. A* **1972**, *5*, 227.
(38) Jungen, Ch.; *Molecular Applications of Quantum Defect Theory*; Taylor and Francis, New York: 1996.
(39) Suzuki, Y.; Suzuki, T. *Mol. Phys.* **2007**, *105*, 1675.
(40) Suzuki, T. *Annu. Rev. Phys. Chem.* **2006**, *57*, 555.
(41) Ng, C. Y. *J. Eelectron. Spectrosc. Relat. Phenom.* **2005**, *142*, 179.
(42) Wallace S.; Dill D. *Phys. Rev. B* **1978**, *17*, 1697.
(43) Lucchese R. R.; Raseev G.; McKoy V. *Phys. Rev. A* **1982**, *25*, 2572.
(44) Wilhelmy, I.; Ackermann, L.; Gorling, A.; Rosch, N. *J. Chem. Phys.* **1994**, *100*, 2808.
(45) Venuti, M.; Stener, M.; Decleva, P. *Chem. Phys. Lett.* **1998**, *234*, 95.
(46) Zare, R. N. *Angular Momentum. Understanding Spatial Aspects in Chemistry and Physics*; Wiley: New York, 1988.